Astronomy
&
Astrophysics

Production of atomic hydrogen by cosmic rays in dark clouds

Marco Padovani[1], Daniele Galli[1], Alexei V. Ivlev[2], Paola Caselli[2], and Andrea Ferrara[3]

[1] INAF – Osservatorio Astrofisico di Arcetri, Largo E. Fermi 5, 50125 Firenze, Italy
    e-mail: padovani@arcetri.astro.it
[2] Max-Planck-Institut für Extraterrestrische Physik, Giessenbachstr. 1, 85741 Garching, Germany
[3] Scuola Normale Superiore, Piazza dei Cavalieri 7, 56126 Pisa, Italy

ABSTRACT

Context. Small amounts of atomic hydrogen, detected as absorption dips in the 21 cm line spectrum, are a well-known characteristic of dark clouds. The abundance of hydrogen atoms measured in the densest regions of molecular clouds can only be explained by the dissociation of H_2 by cosmic rays.
Aims. We wish to assess the role of Galactic cosmic rays in the formation of atomic hydrogen, for which we use recent developments in the characterisation of the low-energy spectra of cosmic rays and advances in the modelling of their propagation in molecular clouds.
Methods. We modelled the attenuation of the interstellar cosmic rays that enter a cloud and computed the dissociation rate of molecular hydrogen that is due to collisions with cosmic-ray protons and electrons as well as fast hydrogen atoms. We compared our results with the available observations.
Results. The cosmic-ray dissociation rate is entirely determined by secondary electrons produced in primary ionisation collisions. These secondary particles constitute the only source of atomic hydrogen at column densities above $\sim 10^{21}$ cm^{-2}. We also find that the dissociation rate decreases with column density, while the ratio between the dissociation and ionisation rates varies between about 0.6 and 0.7. From comparison with observations, we conclude that a relatively flat spectrum of interstellar cosmic-ray protons, such as suggested by the most recent Voyager 1 data, can only provide a lower bound for the observed atomic hydrogen fraction. An enhanced spectrum of low-energy protons is needed to explain most of the observations.
Conclusions. Our findings show that a careful description of molecular hydrogen dissociation by cosmic rays can explain the abundance of atomic hydrogen in dark clouds. An accurate characterisation of this process at high densities is crucial for understanding the chemical evolution of star-forming regions.

Key words. dust, extinction – ISM: clouds – atomic processes – molecular processes
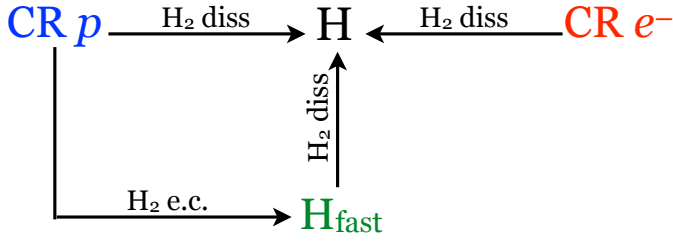
1. Introduction

The formation of molecular hydrogen occurs on dust grains in molecular clouds through the reaction between two hydrogen atoms. Because this is an exothermic process, H_2 is then released into the gas phase. Depending on the position in the cloud (or on the amount of visual extinction measured inward from the cloud edge), two processes determine the destruction of H_2 and the restoration of the atomic form: photodissociation that is due to interstellar (hereafter IS) UV photons, and dissociation due to cosmic rays (hereafter CRs). In the diffuse part of molecular clouds, UV photons regulate the abundance of atomic hydrogen by dissociating H_2, while in the densest parts, IS UV photons are blocked by dust absorption as well as by H_2 line absorption (Hollenbach et al. 1971). In the deepest parts of the cloud, CRs dominate the destruction of molecular hydrogen.

A wealth of studies has been carried out to characterise the origin of the atomic hydrogen component in dense environments (e.g. McCutcheon et al. 1978; van der Werf et al. 1988; Montgomery et al. 1995; Li & Goldsmith 2003; Goldsmith & Li 2005), but the rate of CR dissociation was always assumed to be constant (i.e., independent of the position in the cloud) or was simply neglected. In this paper, we wish to explore the role of CRs in more detail, especially after the latest data release of the Voyager 1 spacecraft (Cummings et al. 2016), which showed that the measured proton and electron fluxes are not able to explain

the values of the CR ionisation rate estimated in diffuse clouds (e.g. Indriolo et al. 2015; Phan et al. 2018). In our previous work (e.g. Padovani et al. 2009, 2013, 2018; Padovani & Galli 2013; Ivlev et al. 2015) we postulated the presence of a low-energy component in the IS CR proton spectrum, with which it is possible to recover the high ionisation rates observed in diffuse clouds.

We treat a cloud as a semi-infinite slab. This simplification is completely justified for our purposes for the following reasons. First, attenuation of IS UV photons occurs in a thin gas layer near the cloud surface (with a visual extinction of $A_V \approx 1-3$ mag), that is, at column densities much lower than those characterising the line-of-sight thickness of a cloud. Second, CRs propagate through a cloud along the local magnetic field. The latter assumption is always valid since the Larmor radius of sub-relativistic CRs is much smaller than any characteristic spatial scale of the cloud (Padovani & Galli 2011) and the correlation length of the magnetic field (Houde et al. 2009). Therefore, regardless of the field geometry, we can measure the coordinate along the local field line and treat this as a one-dimensional problem (Padovani et al. 2018). The CR ionisation rate is then a function of the effective column density, measured along the field line. To facilitate the presentation of our results, we assume the line-of-sight and the effective column densities to be the same. These considerations can be generalised to a slab of a finite thickness by adding IS particles that enter the cloud

Fig. 1. Dissociation diagram showing the three main processes of atomic hydrogen production. Labels "diss" and "e.c." refer to dissociation and electron capture, respectively.

from the opposite side; however, given a strong attenuation, this addition is only important for clouds with column densities of $\approx 10^{22}$ cm^{-2} or lower (increasing the ionisation and dissociation rates in the cloud centre by up to a factor of 2).

The paper is organised as follows: in Sect. 2, we discuss the main processes of H$_2$ dissociation by CR protons, electrons, and fast hydrogen atoms, and compute the resulting dissociation rate as a function of the column density, in Sect. 3, we present equations to compute the fractions of atomic and molecular hydrogen, in Sect. 4, we compare our theoretical findings with available observations, and in Sect. 5, we discuss implications for our outcomes and summarise the most important results.

2. CR dissociation reactions with H$_2$

We considered dissociation processes induced by CR primary and secondary electrons, CR protons, and fast hydrogen atoms colliding with molecular hydrogen. A schematic diagram of different dissociation paths is depicted in Fig. 1.

2.1. Electron impact

Electrons can produce atomic hydrogen by exciting five electronic states of the H$_2$ triplet ($a^3\Sigma_g^+$, $b^3\Sigma_u^+$, $c^3\Pi_u$, $e^3\Sigma_u^+$, and $d^3\Pi_u$), followed by dissociation. While the radiative decay from the state $b^3\Sigma_u^+$ is fully dissociative, the decay from $e^3\Sigma_u^+$ contributes to dissociation at 20%, and dissociation from the other states is negligible. There is also a contribution from the H$_2$ singlet state, but the respective cross section peaks at about 40−50 eV with a maximum value of 3.02×10^{-18} cm^2, which is a factor ≈ 20 lower than the peak value of the triplet-state cross section. Thus, the dissociation cross section by electron impact is given by

$$\sigma^e_{\text{diss}} \simeq \sigma^e_{\text{exc}}(X \rightarrow b^3\Sigma_u^+) + 0.2\sigma^e_{\text{exc}}(X \rightarrow e^3\Sigma_u^+). \quad (1)$$

2.2. Proton impact

Atomic hydrogen can also be produced by protons, by direct dissociation of H$_2$ from the vibrational state $v = 0$. The H$_2$ excitation cross sections by electrons, σ^e_{exc}, and the dissociation cross section by protons, σ^p_{diss}, have been parameterised by Janev et al. (2003) as

$$\sigma(E) = \frac{a}{E^{\alpha_1}} \left[1 - \left(\frac{E_0}{E}\right)^{\alpha_2} \right]^{\alpha_3} \times 10^{-16} \text{ cm}^2, \quad (2)$$

with the energy E in eV. In Table 1, we list the values of factor a, exponents $\alpha_{1,2,3}$, and the energy threshold E_0 for the respective cross sections.
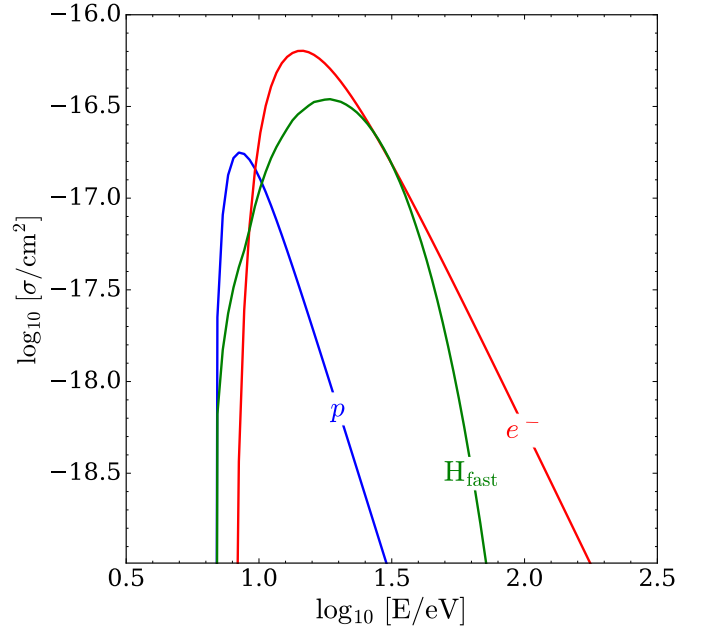
Fig. 2. Energy dependence of the dissociation cross sections by protons (blue), electrons (red), and fast hydrogen atoms (green) colliding with molecular hydrogen.

2.3. Effect of fast hydrogen atoms

Figure 2 shows that dissociation cross sections peak at very low energy, about 8 and 15 eV for protons and electrons, respectively, which means that the processes that regulate the distributions of different species in this energy range require close study. In Appendix A, we demonstrate that CR protons are efficiently neutralised at low energies because of electron capture (see also Chabot 2016). This generates a flux of fast H atoms (hereafter H$_{\text{fast}}$) that in turn creates fast H$^+$ ions (secondary CR protons) through reaction (A.3). We computed the equilibrium distributions of protons and H$_{\text{fast}}$ atoms, finding that below $\approx 10^4$ eV, less than 10% of (non-molecular) hydrogen is in the form of H$^+$ (see Fig. A.2), so that the dissociation by H$_{\text{fast}}$ (reaction A.4) must be taken into account. The corresponding cross section, σ^H_{diss} (Dove & Mandy 1986; Esposito & Capitelli 2009) is also plotted in Fig. 2.

2.4. CR dissociation rate

The rate of dissociation due to primary and secondary CRs and H$_{\text{fast}}$ atoms, occurring at the total column density N, is given by

$$\zeta^k_{\text{diss}}(N) = 2\pi\ell \int j_{\text{k}}(E, N)\sigma^k_{\text{diss}}(E)\text{d}E, \quad (3)$$

where j_{k} is the differential flux of CR particles k, σ^k_{diss} is the dissociation cross section, and $k = p, e, \text{H}_{\text{fast}}$. In the semi-infinite slab geometry, the factor ℓ is equal to 1 for primary CRs and H$_{\text{fast}}$, and equal to 2 for secondary electrons (because the latter are produced isotropically). The final expression for the dissociation rate is obtained by averaging over the pitch-angle distribution of the incident CRs (see Eq. (45) in Padovani et al. 2018).

In the following we assume the same IS CR proton and electron spectra as in Ivlev et al. (2015) and Padovani et al. (2018). For CR protons we adopt two different models: the first, model $\mathscr{L}$, is an extrapolation of the Voyager 1 observations to lower

Table 1. Parameters for the proton dissociation cross section and the (relevant) electron excitation cross sections (Eq. 2).

Reaction	a	α_1	α_2	α_3	E_0 (eV)
$p + H_2 \rightarrow p + H + H$	7.52×10^3	4.64	5.37	2.18	6.72
$e + H_2 \rightarrow e + H_2^*(b^3\Sigma_u^+)$	5.57×10^3	3.00	2.33	3.78	7.93
$e + H_2 \rightarrow e + H_2^*(e^3\Sigma_u^+)$	4.17×10^2	3.00	4.50	1.60	13.0
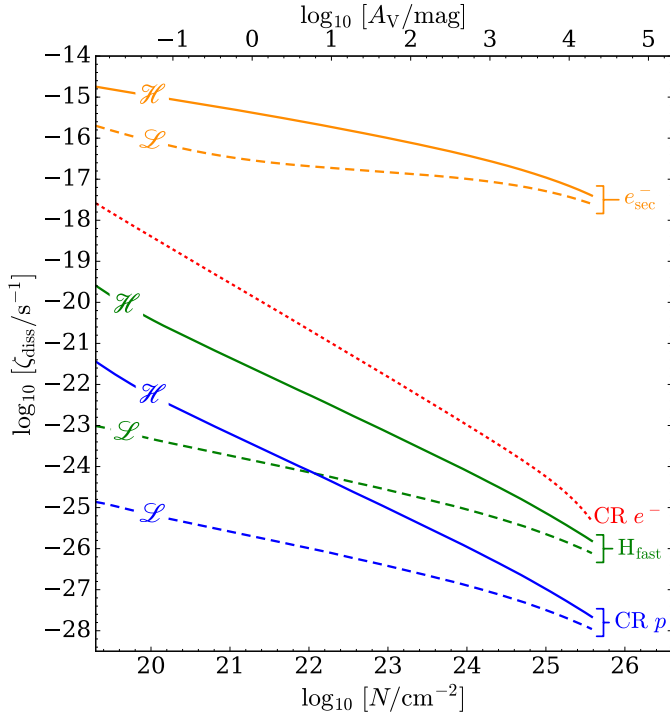
Fig. 3. CR dissociation rate for models $\mathscr{L}$ and $\mathscr{H}$ (dashed and solid lines, respectively) as a function of the total column density of hydrogen (bottom scale) and visual extinction (top scale). The contributions of primary CR protons (blue) and electrons (red dotted), secondary electrons (orange), and fast H atoms (green) are shown.

energies; the second, model $\mathscr{H}$, is characterised by an enhanced flux of low-energy protons with respect to Voyager 1 data. Models $\mathscr{L}$ and $\mathscr{H}$ can be regarded as the lower and upper bound, respectively, of the average Galactic CR proton spectrum, since the corresponding CR ionisation rates encompass the values estimated from observations in diffuse clouds (e.g. Indriolo et al. 2015; Neufeld & Wolfire 2017). For CR electrons, we use a single model based on the latest Voyager results, which show that the electron flux varies at $E \lesssim 100$ MeV as $\propto E^{-1.3}$ (Cummings et al. 2016). Figure 3 shows the partial contributions to the dissociation rate of primary CR protons and electrons, H_{fast} atoms, and secondary electrons. The latter is computed following Eq. (16) in Ivlev et al. (2015). In Fig. 3, we also show the corresponding visual extinction, $A_V = 5.32 \times 10^{-22} (N/\text{cm}^{-2})$. Clearly, ζ_{diss} is entirely dominated by low-energy secondary electrons that are produced during the propagation of primary CRs.

In previous work (e.g. Li & Goldsmith 2003; Goldsmith & Li 2005), ζ_{diss} has usually been assumed to be equal to the CR ionisation rate, ζ_{ion} (which in turn did not depend on N). In Fig. 4 we show that ζ_{diss} and ζ_{ion} exhibit very similar behaviour: they decrease monotonically with N; the ratio ζ_{diss}/ζ_{ion} can be as low as ≈ 0.63 at low column densities ($N \approx 10^{19}$ cm^{-2}), depending on the assumed spectrum of IS CR protons. This

ratio rapidly approaches the constant value of ≈ 0.7, and at $N \gtrsim 10^{22}$ cm^{-2} becomes independent of the column density and the IS proton spectrum. The values of ζ_{diss} and ζ_{ion} are comparable because secondary electrons provide the main contribution to both processes. We note that the ionisation rate was computed by taking into account the presence of H_{fast} atoms (see Eq. (B.1)) that contribute to the production of H_2^+ ions through reaction (A.2) at energies below $\approx 10^4$ eV. However, this process is only marginally important for model $\mathscr{H}$ below $N \approx 10^{21}$ cm^{-2}, and is always negligible for model $\mathscr{L}$ (see Appendix B). Figure 4 also shows the photodissociation rate, $\zeta_{pd} = D_0\chi_a$, computed following Draine (2011).

3. Balance equation

Goldsmith & Li (2005) and Goldsmith et al. (2007) presented a time-dependent modelling of the H abundance in molecular clouds and introduced the concept of the atomic-to-molecular hydrogen ratio, n_H/n_{H_2}, as a clock of the evolutionary stage of a cloud. In particular, Goldsmith & Li (2005) modelled observations of n_H/n_{H_2} in five dark clouds, concluding that the characteristic time required to reach a steady-state n_H/n_{H_2} ratio is close to the cloud ages. In the following, we consider the steady-state solution, keeping in mind that time dependence may still affect the interpretation of the observational data (see Sect. 4).

In steady state, the balance between H_2 formation and destruction processes gives

$$Rnn_H = n_{H_2}(D_0\chi_a + \zeta_{diss}) . \tag{4}$$

Here, $n = n_H + 2n_{H_2}$ is the total volume density of hydrogen, R is the H_2 formation rate coefficient, D_0 is the unattenuated photodissociation rate, χ_a is the attenuation factor for dust absorption and H_2-self shielding, and ζ_{diss} is the CR dissociation rate. In the following we assume $R = 3 \times 10^{-17}$ cm^3 s^{-1} (Jura 1975) and $D_0 = 2 \times 10^{-11}G_0$ s^{-1} (Draine 2011, taking into account a semi-infinite slab geometry), where G_0 is the far-UV (FUV) radiation field in Habing units (Habing 1968). Unless specified otherwise, we adopt $G_0 = 1$. The attenuation factor is usually written in the form

$$\chi_a(N, N_{H_2}) = \chi_{sh}(N_{H_2})e^{-\tau(N)} , \tag{5}$$

where $\chi_{sh}(N_{H_2}) = (10^{14} \text{ cm}^{-2}/N_{H_2})^{0.75}$ is the H_2 self-shielding factor (Tielens 2010, valid for 10^{14} cm$^{-2} \lesssim N_{H_2} \lesssim 10^{21}$ cm^{-2}) and $\tau(N) = \sigma_g N$ is the dust attenuation. Here, $N = N_H + 2N_{H_2}$ is the total column density of hydrogen and $\sigma_g = 1.9 \times 10^{-21}$ cm^2 is the average value of the FUV dust grain absorption cross section for solar metallicity (Draine 2011).

Assuming $n_H/n = dN_H/dN$ and $n_{H_2}/n = dN_{H_2}/dN$, Eq. (4) becomes

$$\frac{dN_{H_2}}{dN} = \left(2 + \frac{D_0\chi_a + \zeta_{diss}}{Rn}\right)^{-1} . \tag{6}$$
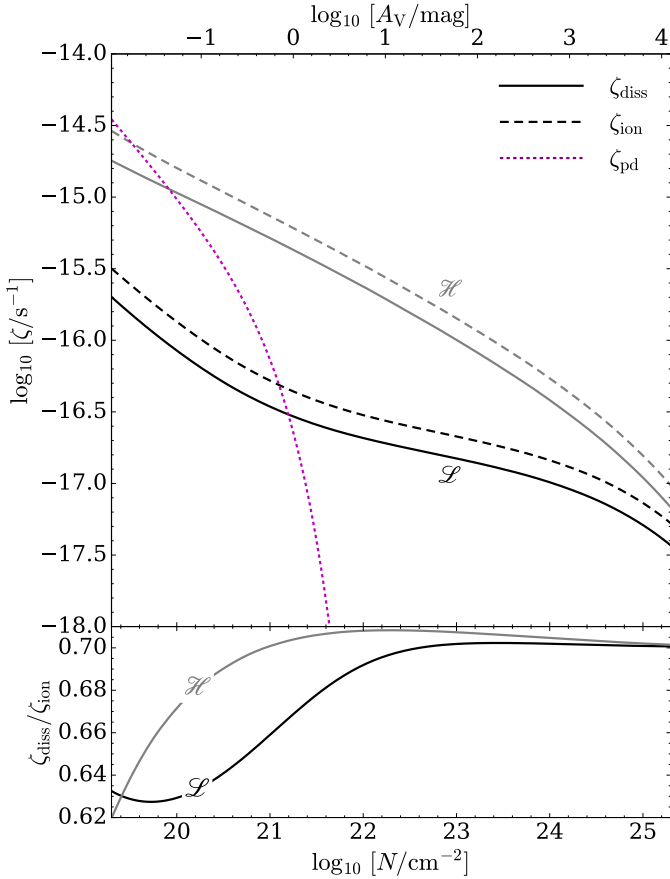
Fig. 4. *Top panel*: CR dissociation rates (ζ_{diss}, solid lines), CR ionisation (ζ_{ion}, dashed lines), and photodissociation (ζ_{pd}, purple dotted line) for models $\mathscr{L}$ (black) and $\mathscr{H}$ (grey), plotted vs. the total column density of hydrogen (bottom scale) and visual extinction (top scale). *Bottom panel*: $\zeta_{\mathrm{diss}}/\zeta_{\mathrm{ion}}$ ratio for the two models.

The fractions of atomic and molecular hydrogen can be expressed as

$$f_{\mathrm{H}} = \frac{n_{\mathrm{H}}}{n_{\mathrm{H}} + n_{\mathrm{H_2}}} = \frac{1 - 2\,\mathrm{d}N_{\mathrm{H_2}}/\mathrm{d}N}{1 - \mathrm{d}N_{\mathrm{H_2}}/\mathrm{d}N}, \tag{7}$$

and

$$f_{\mathrm{H_2}} = 1 - f_{\mathrm{H}} = \frac{\mathrm{d}N_{\mathrm{H_2}}/\mathrm{d}N}{1 - \mathrm{d}N_{\mathrm{H_2}}/\mathrm{d}N}, \tag{8}$$

respectively. In the next section we describe in detail all the processes that contribute to the dissociation of molecular hydrogen.

4. Comparison with observations

Li & Goldsmith (2003) performed a survey of dark clouds in the Taurus-Perseus region, and reported the detection of H I narrow self-absorption features. This allowed them to compute the atomic and molecular hydrogen fraction (Eqs. (7) and (8)). They concluded that a relevant fraction of atomic hydrogen is mixed with H_2 in the densest part of a cloud that is shielded from the IS UV flux.

At high column densities typical of dark clouds, the attenuation factor χ_a in Eq. (4) is so large that the UV photodissociation is inefficient, and the observed $n_{\mathrm{H}}/n_{\mathrm{H_2}}$ ratios can only be explained by CR dissociation. In Sect. 2.4, we showed that $\zeta_{\mathrm{diss}} \approx 0.7\zeta_{\mathrm{ion}}$ at typical column densities of dark clouds ($\approx 10^{22}$ cm^{-2});
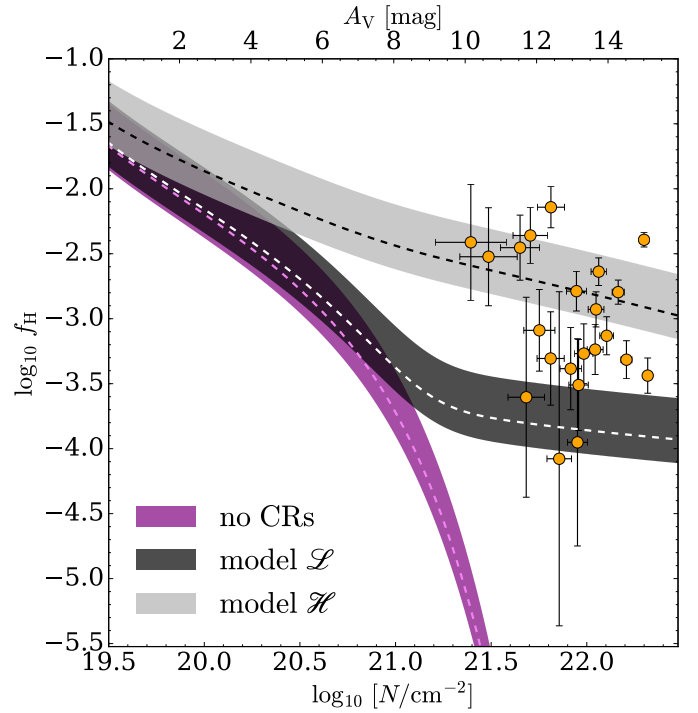
Fig. 5. Atomic hydrogen fraction vs. the total column density of hydrogen (bottom scale) and visual extinction (top scale). Observations from Li & Goldsmith (2003) are shown as solid orange circles. Coloured stripes represent our results for the case of photodissociation only (purple), and models $\mathscr{L}$ (black) and $\mathscr{H}$ (grey). Dashed lines refer to the average value of the total volume density of hydrogen (suggested by Li & Goldsmith 2003).

more importantly, ζ_{diss} is not constant, but decreases with N (e.g. Padovani et al. 2009, 2018).

We computed the fraction of atomic and molecular hydrogen expected at different column densities (Eqs. (7) and (8)) to evaluate the effect of CR dissociation on the abundance of atomic hydrogen in dark clouds. For the total volume density n in Eq. (4), we used the average value of 5×10^3 cm^{-3} computed by Li & Goldsmith (2003), to which we added an error of 2.6×10^3 cm^{-3} (the standard deviation for the observed values).

Figure 5 shows the comparison between our models and the observations by Li & Goldsmith (2003). As expected, UV photodissociation alone cannot explain the observed $n_{\mathrm{H}}/n_{\mathrm{H_2}}$ ratios because of the attenuation at high column densities. More notably, a CR spectrum based on the extrapolation of the Voyager data (model $\mathscr{L}$) fails to reproduce the majority of the observations, and only a spectrum enhanced at low energies (such as model $\mathscr{H}$) can explain this. The latter fact corroborates the need of a low-energy tail in the IS CR flux of protons, also required to explain the high CR ionisation rates in diffuse clouds (e.g. Padovani et al. 2009; Indriolo et al. 2015).

The large spread in the observed values of f_{H} probably reflects a broad variety of environments in dark clouds, including variations in the density and IS UV radiation field, for instance see e.g. Bialy & Sternberg (2016). In this work we assume a H_2 formation rate of $R = 3 \times 10^{-17}$ cm^3 s^{-1} (see Sect. 3). We note that Li & Goldsmith (2003) used $R = 6.5 \times 10^{-18}$ cm^3 s^{-1}, which is a factor of ≈ 5 smaller than our value. A lower R implies a lower ionisation rate needed to reproduce the observations. This explains why, using a constant dissociation rate equal to the ionisation rate of 3×10^{-17} s^{-1}, they found $f_{\mathrm{H}} \approx 1.5 \times 10^{-3}$. However, R is strongly dependent on the condition of each cloud;

for example, in photodissociation regions, where the large abundance of polycyclic aromatic hydrocarbons favours the formation of H_2, R can increase by one order of magnitude (Habart et al. 2004). Variations in the grain size distribution may also change the value of R by a factor of ~3 (Goldsmith & Li 2005). Draine (2011) suggests $R \approx 3 \times 10^{-17} \sqrt{T/70 \, \mathrm{K}} \, \mathrm{cm}^3 \, \mathrm{s}^{-1}$, but even assuming T as low as 10 K, we find $f_H \approx 10^{-3}$ at $N \approx 10^{22}$ cm^{-2} for a Voyager-like spectrum (model $\mathscr{L}$). As a consequence, a higher flux of low-energy CR protons (model $\mathscr{H}$) is still needed to explain the higher n_H/n_{H_2} ratios. This conclusion remains unchanged even if G_0 is increased by up to two orders of magnitude, since the UV field is exponentially attenuated in the range of column densities of the observed dark clouds (2×10^{21} cm$^{-2} \lesssim N \lesssim 2 \times 10^{22}$ cm^{-2}).

We also recall that as mentioned in Sect. 3, some of the observed clouds may not necessarily have reached a steady-state n_H/n_{H_2} ratio (Goldsmith & Li 2005; Goldsmith et al. 2007). In this case, model $\mathscr{L}$ could not be completely ruled out because if these clouds are younger, they will have a higher n_H/n_{H_2} ratio than predicted by our steady-state assumption.

5. Discussion and conclusions

Dissociation of H_2 into atomic hydrogen by CRs in dark clouds can have important consequences for the chemical evolution of dense regions in the clouds. Atomic hydrogen is the most mobile reactive species on the surface of bare dust grains and icy mantles, and therefore it is crucial to accurately determine its abundance. The higher f_H values predicted in this work imply a more efficient hydrogenation of molecular species on grain surfaces. In particular, hydrogenation of CO, which freezes out onto grains at densities above a few 10^4 cm^{-3} (e.g. Caselli et al. 1999), follows the sequence (e.g. Tielens & Hagen 1982)

$$CO \xrightarrow{H} HCO \xrightarrow{H} H_2CO \xrightarrow{H} H_3CO \xrightarrow{H} CH_3OH . \qquad (9)$$

This leads to efficient production of formaldehyde (H_2CO) and methanol (CH_3OH; Vasyunin et al. 2017) on very short timescales. Hence, even if dissociation by energetic particles takes place, CO cannot be returned to the gas phase because it is rapidly converted into methanol. If the products of dissociation do not move very far from their formation site (Shingledecker et al. 2018), methanol is ejected from the surface because the exothermicity of chemical reactions (9) is partially channelled into kinetic energy through a process known as reactive desorption (Garrod et al. 2007). On the other hand, ammonia (NH_3), which is synthesised onto grains through the hydrogenation sequence (e.g. Hiraoka et al. 1995; Fedoseev et al. 2015)

$$N \xrightarrow{H} NH \xrightarrow{H} NH_2 \xrightarrow{H} NH_3 , \qquad (10)$$

can, in principle, return to the gas phase upon surface dissociation followed by reactive desorption. These considerations could help in explaining the observational evidence that NH_3 (unlike CO) does not appear to deplete towards the central regions of dense cores, despite its high binding energy. To verify this hypothesis, the consequences of an enhanced abundance of atomic hydrogen in chemical models need to be evaluated.

We point out that CR dissociation is not only limited to H_2, but could occur for other molecular species as well, both in the gas phase and on/in ices mantles, with potentially significant consequences in the chemical composition of dense cloud cores and dark clouds.

To summarise, we studied the role of CRs in determining the fractional abundance of atomic hydrogen in dark clouds. The main results are listed below.

(*i*) The CR dissociation rate, ζ_{diss}, is primarily determined by secondary electrons produced during the primary CR ionisation process. These secondary electrons can efficiently dissociate H_2 and represent the only source of atomic hydrogen at column densities higher than $\approx 10^{21}$ cm^{-2}, regulating the n_H/n_{H_2} ratio in dark clouds.

(*ii*) ζ_{diss} entering the balance Eq. (4) is not equal to the ionisation rate ζ_{ion}, as assumed in some previous work. We find that the ratio $\zeta_{\mathrm{diss}}/\zeta_{\mathrm{ion}}$ varies between ≈ 0.63 and ≈ 0.7, depending on the column density range, while ζ_{ion} is a decreasing function of the column density.

(*iii*) Even given the uncertainties in the values of H_2 formation rate, temperature, total hydrogen volume density, and IS UV radiation field for each cloud, only a CR proton spectrum enhanced at low energies (such as our model $\mathscr{H}$) is capable of reproducing the upper values of measured f_H under the assumption of steady state. We note that neither model $\mathscr{L}$ nor model $\mathscr{H}$ is able to reproduce the entire set of observational data: the spread in the values of f_H at any given column density must be attributed to time dependence or to individual characteristics of each cloud. For example, tangled magnetic field lines and/or higher volume densities would result in a stronger CR attenuation and therefore in a lower f_H.

(*iv*) An accurate description of H_2 dissociation in dense environments is essential because many chemical processes (such as CO hydrogenation and its depletion degree onto dust grains, or formation of complex organic molecules) critically depend on the abundance of atomic hydrogen.

References

Bialy, S., & Sternberg, A. 2016, ApJ, 822, 83
Caselli, P., Walmsley, C. M., Tafalla, M., Dore, L., & Myers, P. C. 1999, ApJ, 523, L165
Chabot, M. 2016, A&A, 585, A15
Cummings, A. C., Stone, E. C., Heikkila, B. C., et al. 2016, ApJ, 831, 18
Dove, J. E., & Mandy, M. E. 1986, ApJ, 311, L93
Draine, B. T. 2011, Physics of the Interstellar and Intergalactic Medium (Princeton: Princeton University Press)
Esposito, F., & Capitelli, M. 2009, J. Phys. Chem. A, 113, 15307
Fedoseev, G., Ioppolo, S., Zhao, D., Lamberts, T., & Linnartz, H. 2015, MNRAS, 446, 439
Garrod, R. T., Wakelam, V., & Herbst, E. 2007, A&A, 467, 1103
Goldsmith, P. F., & Li, D. 2005, ApJ, 622, 938
Goldsmith, P. F., Li, D., & Krčo M. 2007, ApJ, 654, 273
Habart, E., Boulanger, F., Verstraete, L., Walmsley, C. M., & Pineau des Forêts, G. 2004, A&A, 414, 531
Habing, H. J. 1968, Bull. Astron. Inst. Netherlands, 20, 120
Hiraoka, K., Yamashita, A., Yachi, Y., et al. 1995, ApJ, 443, 363
Hollenbach, D. J., Werner, M. W., & Salpeter, E. E. 1971, ApJ, 163, 165
Houde, M., Vaillancourt, J. E., Hildebrand, R. H., Chitsazzadeh, S., & Kirby, L. 2009, ApJ, 706, 1504
Indriolo, N., Neufeld, D. A., Gerin, M., et al. 2015, ApJ, 800, 40
Ivlev, A. V., Padovani, M., Galli, D., & Caselli, P. 2015, ApJ, 812, 135
Janev, R. K., Reiter, D., & Samm, U. 2003, Collision Processes in Low-Temperature Hydrogen Plasmas (Jülich, Germany: Forschungszentrum, Zentralbibliothek), 188
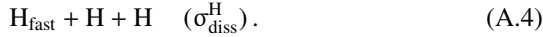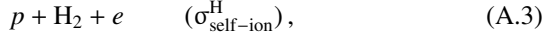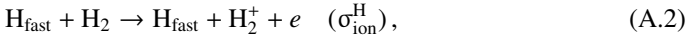
Jura, M. 1975, ApJ, 197, 575

Kunc, J. A., & Soon, W. H. 1991, J. Chem. Phys., 95, 5738

Li, D., & Goldsmith, P. F. 2003, ApJ, 585, 823

McCutcheon, W. H., Shuter, W. L. H., & Booth, R. S. 1978, MNRAS, 185, 755

Montgomery, A. S., Bates, B., & Davies, R. D. 1995, MNRAS, 273, 449

Neufeld, D. A., & Wolfire, M. G. 2017, ApJ, 845, 163

Padovani, M., & Galli, D. 2011, A&A, 530, A109

Padovani, M., & Galli, D. 2013, in Cosmic Rays in Star-Forming Environments, eds. D. F. Torres, & O. Reimer, Astrophysics and Space Science Proceedings, 34, 61

Padovani, M., Galli, D., & Glassgold, A. E. 2009, A&A, 501, 619

Padovani, M., Hennebelle, P., & Galli, D. 2013, A&A, 560, A114

Padovani, M., Ivlev, A. V., Galli, D., & Caselli, P. 2018, A&A, 614, A111

Phan, V. H. M., Morlino, G., & Gabici, S. 2018, MNRAS, 480, 5167

Phelps, A. V. 1990, J. Phys. Chem. Ref. Data, 19, 653

Rudd, M. E., Goffe, T. V., Dubois, R. D., Toburen, L. H., & Ratcliffe, C. A. 1983, Phys. Rev. A, 28, 3244

Rudd, M. E., Kim, Y.-K., Madison, D. H., & Gallagher, J. W. 1985, Rev. Mod. Phys., 57, 965

Shingledecker, C. N., Tennis, J., Le Gal, R., & Herbst, E. 2018, ApJ, 861, 20

Stier, P. M., & Barnett, C. F. 1956, Phys. Rev., 103, 896

Tielens, A. G. G. M. 2010, The Physics and Chemistry of the Interstellar Medium (Cambridge: Cambridge University Press)

Tielens, A. G. G. M., & Hagen, W. 1982, A&A, 114, 245

van der Werf, P. P., Goss, W. M., & Vanden Bout P. A. 1988, A&A, 201, 311

van Zyl, B., Le, T. Q., & Amme, R. C. 1981, J. Chem. Phys., 74, 314

Vasyunin, A. I., Caselli, P., Dulieu, F., & Jiménez-Serra, I. 2017, ApJ, 842, 33

Appendix A: Equilibrium distribution of protons and H_fast atoms at low energies

Because of the process of electron capture at low energies, CR protons interacting with H_2 are efficiently neutralised,

$$p + H_2 \rightarrow H_2^+ + H_{fast} \quad (\sigma^p_{e.c.}), \qquad (A.1)$$
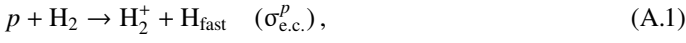
creating fast H atoms. In parentheses we list the cross section of the respective process. At the same time, H_{fast} atoms reacting with H_2 yield

$$H_{fast} + H_2 \rightarrow H_{fast} + H_2^+ + e \quad (\sigma^H_{ion}), \qquad (A.2)$$

$$p + H_2 + e \qquad (\sigma^H_{self-ion}), \qquad (A.3)$$

$$H_{fast} + H + H \quad (\sigma^H_{diss}). \qquad (A.4)$$

The electron capture by protons, reaction (A.1), and the reaction of H_{fast} self-ionisation, reaction (A.3), are catastrophic processes, since the respective projectile particles disappear after such collisions. The reactions of H_2 ionisation and dissociation by H_{fast} atoms, reactions (A.2) and (A.4), respectively, are continuous loss processes, where the projectile kinetic energy decreases only slightly after each collision. The efficiency of continuous energy losses is generally characterised by the projectile stopping range (see, e.g. Padovani et al. 2009).

For our calculations, $\sigma^p_{e.c.}$ is taken from Rudd et al. (1983), σ^H_{ion} is adopted from Phelps (1990) and Kunc & Soon (1991), $\sigma^H_{self-ion}$ is computed by Stier & Barnett (1956), van Zyl et al. (1981), and Phelps (1990), and σ^H_{diss} is taken from Dove & Mandy (1986) and Esposito & Capitelli (2009). In Fig. A.1, we plot the cross sections and the inverse of the proton stopping range, R_p^{-1}, versus the respective projectile energy. We see that $\sigma^p_{e.c.}$ is much larger than R_p^{-1} for 10^2 eV $\lesssim E \lesssim 10^5$ eV, which implies that continuous loss processes cannot significantly affect the balance between protons and H_{fast} atoms at these energies. The equilibrium ratio of the H_{fast} and proton fluxes is then given by

$$\frac{j_{H_{fast}}}{j_p} \approx \frac{\sigma^p_{e.c.}}{\sigma^H_{self-ion}}. \qquad (A.5)$$

This allows us to calculate the fractions of H_{fast} atoms,

$$f_{H_{fast}} = \frac{j_{H_{fast}}}{j_{H_{fast}} + j_p} = \frac{\sigma^p_{e.c.}}{\sigma^p_{e.c.} + \sigma^H_{self-ion}}, \qquad (A.6)$$

and protons, $f_p = 1 - f_{H_{fast}}$. Figure A.2 shows that for energies below $\approx 10^4$ eV, only less than 10% of non-molecular hydrogen is in the form of protons. This means that H_2 ionisation at these energies is dominated by H_{fast} atoms via reaction (A.2).

Appendix B: Ionisation by H_fast atoms

As shown in Appendix A, the ionisation at energies below $\approx 10^4$ eV is mostly driven by H_{fast} atoms. To take this effect into account, we use the following expression for the H_2 ionisation rate by CR protons:

$$\zeta^p_{ion}(N) = 2\pi \int \left\{ j_p(E, N) \left[\sigma^p_{ion}(E) + \sigma^p_{e.c.}(E) \right] \right. \qquad (B.1)$$
$$\left. + j_{H_{fast}}(E, N) \sigma^H_{ion}(E) \right\} dE,$$

where σ^p_{ion} is the H_2 ionisation cross section by proton impact (Rudd et al. 1985). It turns out, however, that the difference
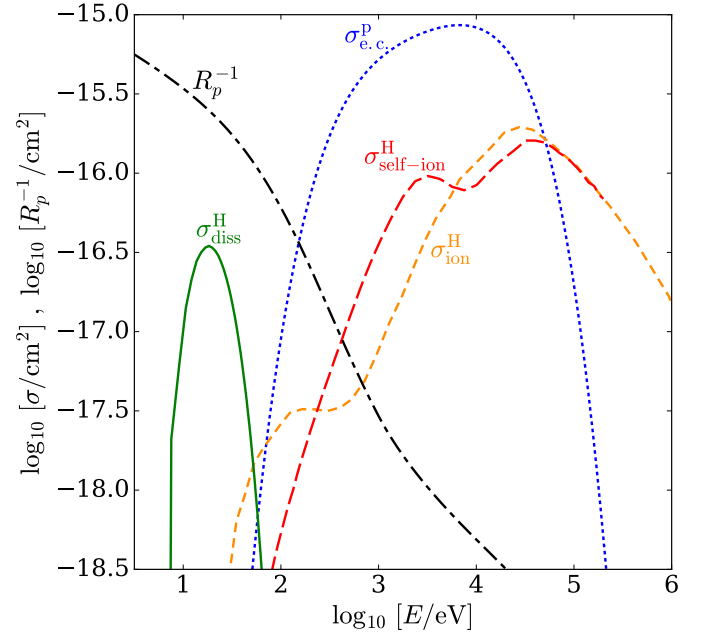
Fig. A.1. Cross sections of processes governing equilibrium distributions of protons and fast hydrogen atoms at low energies: electron capture by p (A.1, dotted blue line), ionisation of H_2 by H_{fast} (A.2, short dashed orange line), self-ionisation of H_{fast} (A.3, long dashed red line), and H_2 dissociation by H_{fast} (A.4, solid green line). The inverse of the proton stopping range, R_p^{-1}, is also plotted (black dot-dashed line).
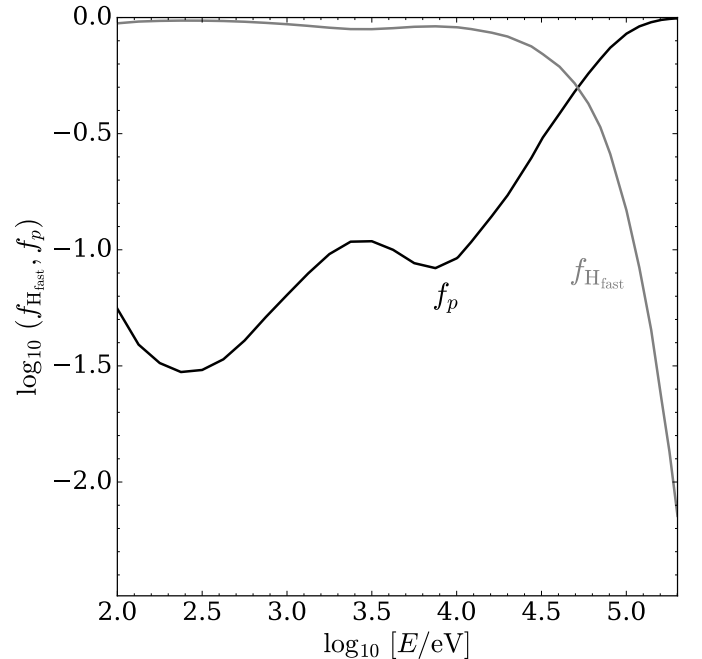
Fig. A.2. Fraction of non-molecular hydrogen in neutral ($f_{H_{fast}}$) and ionised (f_p) form as a function of the energy.

between the ionisation rates computed from Eq. (B.1) taking into account Eq. (A.5) and assuming $j_{H_{fast}} = 0$ is very small: for $N \approx 10^{19}$ cm^{-2}, the difference is $\approx 5\%$ and $\approx 40\%$ for models $\mathscr{L}$ and $\mathscr{H}$, respectively. At higher column densities, it rapidly decreases and becomes negligible for both models above $\approx 10^{21}$ cm^{-2}. This result justifies the assumption $j_{H_{fast}} = 0$ made previously for calculating the ionisation.